American Mineralogist, Volume 104, pages 966–972, 2019

A topological model for defects and interfaces in complex crystal structures

J.P. Hirth[1], Jian Wang[2], and Greg Hirth[3,*]

[1]Emeritus Professor, Ohio State and Washington State Universities, 546 S. Park Centre Avenue, Green Valley, Arizona 54614, U.S.A.
[2]Mechanical and Materials Engineering Department, University of Nebraska-Lincoln, Lincoln, Nebraska 68588, U.S.A.
[3]Department of Geological Sciences, Brown University, Providence, Rhode Island 02912, U.S.A.

Abstract

A topological model (TM) is presented for the complex crystal structures characteristic of some minerals. We introduce a tractable method for applying the TM to characterize defects in these complex materials. Specifically, we illustrate how structural groups, each with a motif containing multiple atoms, provide lattices and structures that are useful in describing dislocations and disconnections in interfaces. Simplified methods for determining the shuffles that accompany disconnection motion are also described. We illustrate the model for twinning in albite owing to its potential application for constraining the rheological properties of the crust at conditions near the brittle-plastic transition, where plagioclase is a major constituent of common rock types. While deformation twins in plagioclase are often observed in crustal rocks, the interpretation of the stress states at which they form has not advanced. The concept of structural groups makes an analysis of the twinning process easier in complex minerals and explicitly predicts the interface structure of the deformation twins.

Keywords: Twinning, mineral, structural group, dislocations, disconnections, topological model

Introduction

Topological theory, based on crystal symmetry with added symmetry elements at interfaces (Pond and Vlachavas 1983), was developed to describe interfaces and defects in crystals (Pond 1989). It was expanded to include a formal description of defects called disconnections (Hirth and Pond 1996). The topological model (TM) entails the application of these ideas to describe dislocations and disconnections at interfaces, including those that provide the mechanism for growth of a phase normal to the interface (Pond et al. 2007). The same defects account for interface structure and misfit accommodation. While almost all applications have dealt with simple metals and simple compounds (e.g., Medlin and Yang 2012), the TM has many potential applications in Earth and planetary sciences, for a wide range of minerals. However, there are added factors that must be considered for more complicated minerals (i.e., with low symmetry and/or a large number of atoms in the unit cell) such as the plagioclase feldspars. Here, we review the topological model and then introduce new concepts useful in the application of the TM to more complicated mineral structures.

Disconnections are linear interface defects with both a step character and dislocation components characterized by the Burgers vector. Motion of the disconnection can be envisioned to occur by a simple engineering shear associated with motion of the dislocation part, and local rearrangements of atoms (shuffles) associated with motion of the step part. These components of the TM and a view of a disconnection are illustrated in Appendix A[1] for the case of a twin in a simple cubic structure. In metals, step heights are small and shuffles are either absent or simple. Minerals often have complex structures containing many atoms, so step heights and corresponding Burgers vectors can be large and the associated shuffles are numerous. To facilitate application of the TM to these complex mineral structures, we propose the concept of a lattice of structural groups and show that this yields the Burgers vector in the TM description. While these ideas are general and can be extended to other processes such as phase transformations and grain boundary sliding (as outlined in the discussion), we introduce these concepts for twinning, using the example of low albite.

Defect properties can be determined by circuit mapping (e.g., the familiar Burgers circuits for dislocations) or by line integrals of symmetry elements. These two techniques were compared in Pond and Hirth (1994) and shown to give equivalent results for defects in twinning and phase transformations, where translation and rotation are the principal symmetry elements. For complex crystal structures, the new concept of a lattice of structural groups makes the circuit mapping technique significantly more tractable. Our focus is on disconnections, interface defects that provide the mechanism for shear-type phase transformation and twinning (reviewed in Hirth et al. 2013, 2016) and grain boundary processes (reviewed in Han et al. 2018). More general symmetry considerations and other types of defects are treated in Pond (1989).

Reference spaces

As reviewed in Howe et al. (2009), early work indicated that transformation defects have step character. Building on the early work, the TM precisely defined the Burgers vector and step height of a disconnection in reference spaces. In the next sections, we describe three perfect reference spaces in the TM, analogous to reference structures for the familiar Burgers circuits for dislocations (Anderson et al. 2017). The volume

* E-mail: Greg_Hirth@brown.edu

0003-004X/19/0007–966$05.00/DOI: https://doi.org/10.2138/am-2019-6892

transformed when the disconnection moves by one repeat distance defines an exchange cell (e-cell) that contains all displacements associated with the transformation.

The coherent dichromatic pattern

The fundamental crystal structure of interfaces is a dichromatic arrangement that superposes the lattices of the two crystals on either side of the interface; by convention, we refer to these as the matrix μ and product λ lattices (Supplemental[1] Fig. A1b). The first reference space is the coherent dichromatic pattern (CDP), which is the superposition of the Bravais lattices of the two crystals. A perfect twin boundary is naturally coherent, but we retain the coherent modifier to emphasize that the same reference applies to facets on twin boundaries and to phase transformations, where coherency stresses are present at the interface. The origin of the CDP is at a maximum symmetry, coincident lattice point on a coincident site plane, e.g., the twin plane. In detail, the CDP is more general than the coincidence site lattice in that there is no need for registry in the direction normal to the interface. The symmetry of the CDP is the union of that of the two component crystals extended by an anti-symmetry element [designated with a prime (′)] unique to the pattern (Pond 1989). In the resulting dichromatic space group, some of the point symmetry elements are coincident and some are anti-symmetric. For an example of the latter, all perfect twins have m′ mirror symmetry. Several examples of CDPs in simple metals are given in Hirth et al. (2013). In contrast, numerous minerals have unit cells containing many atoms. In the following, we show paired reference spaces in CDPs for a simple cubic lattice and for the example of a twin in low albite.

The composition of low albite is ($NaAlSi_3O_8$), and its conventional unit cell is shown in Figure 1. The lattice parameters are a = 0.814 nm, b = 1.2785 nm, and c = 0.7158 nm. The triclinic angles are α = 94.2°, β = 116.6°, and γ = 87.7°. The crystal structure entails a C_i point group and a $C1$-$P\bar{1}$ space group, triclinic with a center of inversion and a basis of four, with indices (hkl). As discussed in Hahn and Klapper (2006), Wenk and Bulakh (2016), and Ribbe (1974), this is a large unit cell selected to parallel the $C1$ monoclinic structure of orthoclase. An alternate (smaller) $C1$ unit cell is shown in red in Figure 2, with indices $(hkl)^0$. The lattice parameters are a^0 = 0.814 nm, b^0 = 0.7716 nm, and c^0 = 0.7158 nm. The triclinic angles are α = 107.27°, β = 116.61°, and γ = 55.87°. From a defect viewpoint, the vectors in the small cell represent possible perfect Burgers vectors. For example, when considering Burgers vectors in plagioclase (e.g., Stünitz et al. 2003) using the larger conventional cell, the vectors ½ [110] and ½[1$\bar{1}$0] are perfect Burgers vectors (i.e., [010] and [0$\bar{1}$0]) when using the smaller cell (Fig. 2).

The CDP for albite is shown in Figure 3. Translation vectors $\mathbf{t}_\mu$ and $\mathbf{t}_\lambda$, with a common origin, connect lattice sites. For twinning and many phase transformations, the circuits in the topological theory reduce to the limiting form of the translation vectors in the two lattices (Pond 1989). Then the Burgers vectors **b** for dislocation components of disconnections or for interface dislocations are given by

$$\mathbf{b} = \mathbf{t}(\lambda) - \mathbf{t}(\mu). \quad (1)$$

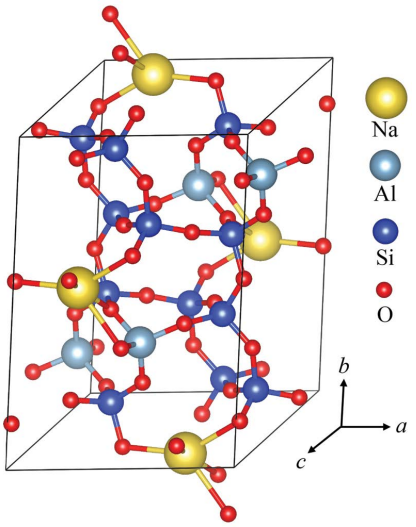

FIGURE 1. Conventional unit cell of low albite. (Color online.)

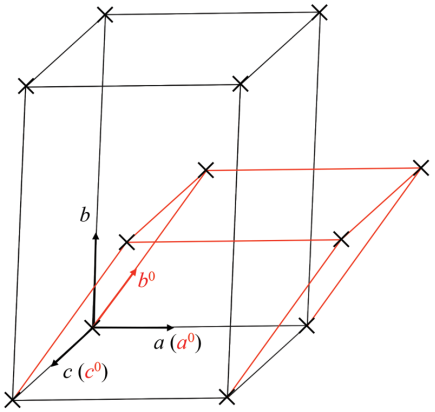

FIGURE 2. Conventional crystal lattice in black. Alternate (smaller) lattice in red. (Color online.)

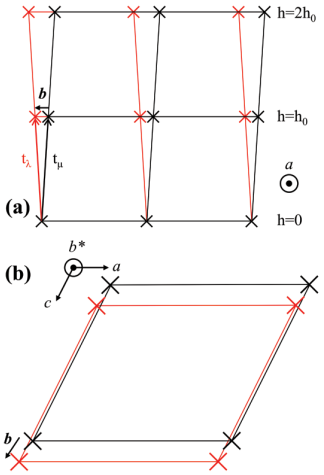

FIGURE 3. Coherent dichromatic pattern (CDP) for an [001] (010) twin in albite. Translation vectors and **b** shown for an $h = h_0$ disconnection. (**a**) Projection along [$\bar{1}$00]. (**b**) Projection along the normal to (0$\bar{1}$0). (Color online.)

Disconnections comprise a dislocation component ***b*** and a step component with height h. In general, the height is given by

$$h = ih_0 \quad (2)$$

where i is an integer and h_0 is equal to the interplanar spacing d of twin (or terrace) planes. Figure 4 shows how a disconnection could be formed from crystals with free surfaces containing steps. The step height of the disconnection is the smaller of h_λ and h_μ. Disconnections separate low-index terraces and their motion provides the mechanism for growth normal to the terraces. The specific disconnection properties are selected so that the structure of the terraces on either side of the defect are identical. The Burgers vector and step height for a specific disconnection with $h = h_0$ are included in Figure 4. Thus, some disconnection properties, **b** and h, are directly determinable from the CDP.

The coherent dichromatic complex

The second reference structure is the coherent dichromatic complex (CDC). The CDC is the superposition of the μ and λ crystal structures and includes the local atomic motif (formally the point group) at a lattice site. Thus, the CDC is a space group that often has lower symmetry than the CDP. The total displacements, $\mathbf{u}(\lambda)$ and $\mathbf{u}(\mu)$, accompanying twinning are depicted in the CDC. The displacement of a given atom is the sum of the shear displacement associated with the dislocation component and the local shuffle displacement that completes the transformation. A simple example of shuffles is shown in Supplemental[1] Figure A1. In most cases, the CDC has coincident symmetry, and we write the displacements as $\mathbf{u}^0(\lambda)$ and $\mathbf{u}^0(\mu)$. In some cases, the two structures comprising the CDC can be offset uniformly by a vector **p** as a consequence of interfacial free energy minimization, with the consequences discussed in Appendix A[1]. Both the μ and λ atoms are displaced by **p** in the e-cell, so the portion of the shuffles associated with **p** cancels. For this reason and because **p** is rarely measured and, when present, is often very small, we neglect it here, so that $\mathbf{u}^0(\mu) = 0$. Then, the shuffles of a given atom are determined by analysis of $\Delta\mathbf{u}$ in the CDC and are given by:

$$\mathbf{s} = \mathbf{u}^0(\lambda) - \mathbf{u}^0(\mu) - \mathbf{b} = \mathbf{u}^0(\lambda) - \mathbf{b}. \quad (3)$$

Alternatively, a shifted dichromatic complex (SDC), where **b** is subtracted from $\mathbf{u}^0(\lambda)$ (Appendix A[1] and Supplemental Fig. A1c) is useful in describing shuffles. The displacements of a given atom in the SDC are those associated only with the shuffles, $\mathbf{u}(\lambda) = \mathbf{u}^0(\lambda) - \mathbf{b}$. Hence, the same shuffles are given by

$$\mathbf{s} = \mathbf{u}(\lambda). \quad (4)$$

Similarly, if the two lattices rotate as a consequence of transformation, the Burgers vectors and shuffles are represented in a rotated RCDP or RDC, respectively (Hirth et al. 2013).

Here we illustrate how the concept of structural groups facilitates the characterization of defects. A unit cell comprised of structural group dipoles is shown in Figure 5a. The motifs of a structural group dipole in the atomic CDC are depicted in Figure 5b. Figure 5c is a rotated view of the motifs with the

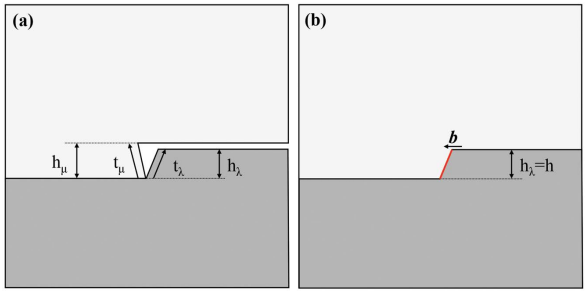

FIGURE 4. Schematic of disconnection. (**a**) Two free surfaces, with translation vectors and h labeled, are joined to create coherent terraces bounding a disconnection (**b**), with **b** shown for $h = h_\lambda$. (Color online.)

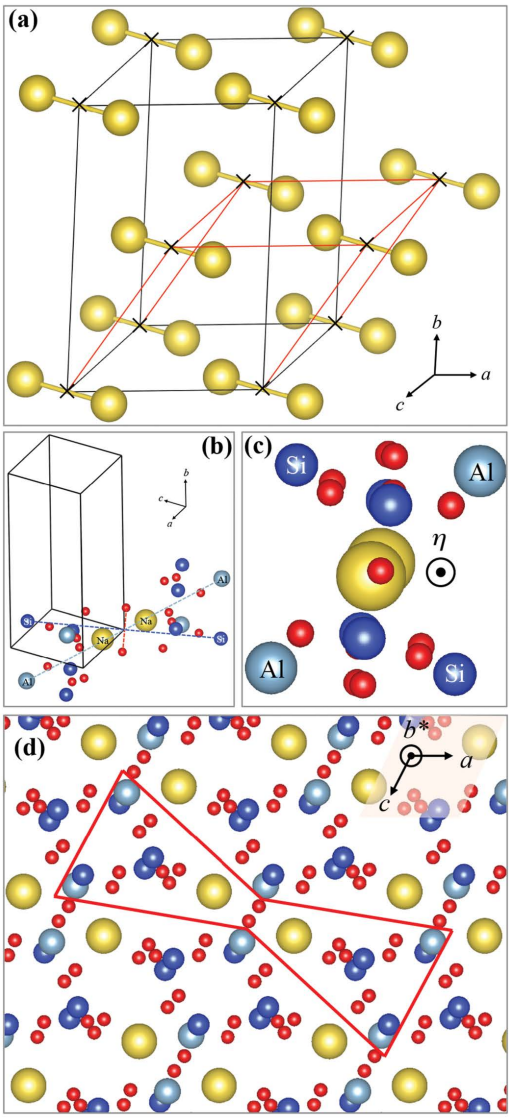

FIGURE 5. (**a**) Unit cell of structural group dipoles. (**b**) Atomic motif of one structural group dipole. (**c**) Projection of panel **b** normal to the twinning direction. (**d**) Projection of panel **b** normal to (010). (Color online.)

twinning direction (η) pointing toward the viewer. The unit cell shown in Figure 5a comprises structural group dipoles centered on cell corners. In both Figures 5a and 5b, the dipoles represent the matrix part of the e-cell: the smallest repeating unit of transformation. As seen in Figure 5b, all atoms occur in pairs with their midpoints at the center of the pair at the same position as the center of the structural group dipole. Hence, the atom pairs also exhibit inversion symmetry. The cell of structural groups is triclinic $P\bar{1}$ with a basis of two. A portion of the CDC is presented in Figure 6. To maintain twin symmetry, the structural group dipoles are displaced in the [010] direction, producing a rotation. The rotation can be represented by a vector $\mathbf{R} = \mathbf{n}\theta$, where **n** is a unit vector along the axis of rotation, perpendicular to the line connecting the dipole members, and θ is the angle of rotation in the plane normal to **n**. For lower albite, **n** = [–0.0432 0 1] and θ = 8.4°. Figure 6a shows that the component of **R** normal to (010) is zero as a structural group moves from the matrix to the twin. However, the out-of-plane rotation is non-zero (Fig. 6b). The **R** vector lies in the (010) plane, with components (R_1, 0, R_3). Hence, for the $h = 1$ albite twin, all shuffles are associated with this rotation, i.e., the entire unit in Figure 6a rotates during the twin transformation. The use of structural groups simplifies the analysis of shuffles, which otherwise would be difficult.

We split the shuffle analysis for albite into several stages. The CDC for structural groups is shown in Figure 6. A depiction of the full CDC would be too complicated, so we show the matrix and the twin separately and deduce the CDC or SDC from these figures. Figures 7a, 7b, and 7c show the matrix, a portion of the matrix sheared but not shuffled, and the true twin, respectively. All are projected along $[\bar{1}0\bar{1}]_0 = [\bar{1}0\bar{1}]$, which is very close to –η.

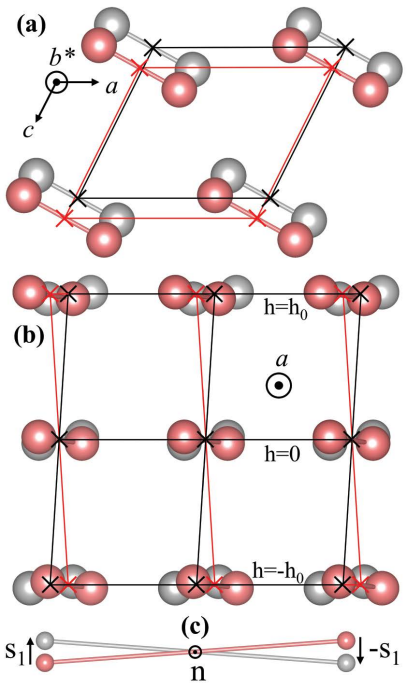

FIGURE 6. CDC for structural groups viewed along *a* and normal to the (010) plane. Rotation of the structural group dipole in the CDC also shown. (Color online.)

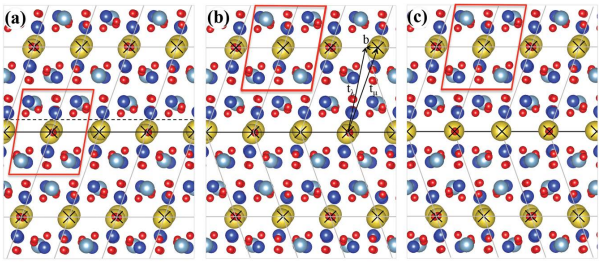

FIGURE 7. (**a**) Repeat unit of two $(010)^0$ planes viewed along $[\bar{1}0\bar{1}]^0$. Solid line will become the twin symmetry plane and the dashed line will become the twin interface. Matrix part of e-cell is enclosed in red. (**b**) Structure of panel **a** is sheared by **b** above the twin boundary, but no shuffles are imposed. In panel **b**, shuffles are added to the matrix part of the e-cell of panel **a**. The extension of the e-cell to encompass the entire region above the twin plane creates the CDC. In panel **c**, the matrix part of the e-cell is in the SDC, with **b** subtracted from panel **b**. (Color online.)

Here, **b** has an out-of-plane component, which is already known from the CDP. One can imagine the SDP by extending the lattices in Figure 7b and deducing the displacements that create the true twin shown in Figure 7c. In the creation of the true twin, the net result of the shuffles is to rotate the motif dipole in Figure 5b by the same angle θ as the structural groups in Figure 5a. This accomplishes one increment of transformation. The shuffles are of two types: exchanges and shifts. The exchange-type shuffles are apparent in the SDC of Figure 7c, or, less straightforwardly, from the CDC of Figure 7b. For the SDC the final structure after shuffling is equivalent to the rotation of the dipole illustrated in Figure 5a about **n** by the same angle as the structural group dipole in Figure 5b. Viewing the dipole in Figures 5c and 5d together with Figure 7b, one sees that most of the Si atoms and all of the O atoms undergo small shifts and some small exchanges. The lengths of the shuffle vectors range from 0.01 to 0.06 nm.

The end-members of the dipole undergo much larger shuffles. Figure 8a shows just the end arrangement of the dipole. To satisfy the mirror symmetry, these Si and Al toms must switch positions in the dipole. The specific view of a portion of the SDC along the dipole axis in Figure 8b shows that these shuffles are large (0.26 to 0.46 nm), roughly an order of magnitude larger than the other shuffles. These are so large that it may be energetically favorable for the Si and Al atoms to shuffle to the wrong type of site as in Figure 8c, creating anti-site defects and disorder. These would have much smaller shuffles, 0.06 nm, of the order of the smaller shifts of oxygen and the Si atoms other than the end-members. The resulting structure would be a pseudo-twin as depicted in Figure 9. The shuffles nominally parallel to the interface are more probable. They are shorter, which means that their self-energy is smaller. Also, they are less likely to produce local, nonlinear displacements normal to the interface, implying a smaller contribution to the activation energy for disconnection motion.

In general, if shuffles are incomplete, there could be two levels of pseudo-twin formation. First, no shuffles could accompany disconnection motion, with all later occurring by thermal relaxation. Second, the smaller shift-type shuffles could accompany disconnection motion, with only the exchange-type shuffles then occurring by thermal relaxation. Both are possible, since the atomistic simulation of the relaxation of an ideal albite twin by

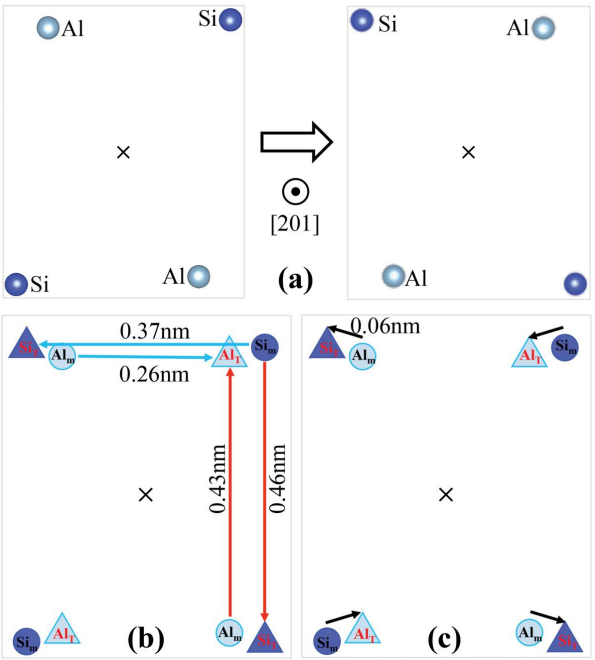

FIGURE 8. (**a**) Atoms at the ends of the structural group dipoles in the e-cell in Figure 5b viewed along the dipole axis. The atoms must shuffle as shown the satisfy mirror symmetry. (**b**) Specific shuffles in a portion of the SDC. (**c**) Shorter shuffles, creating anti-site defects. (Color online.)

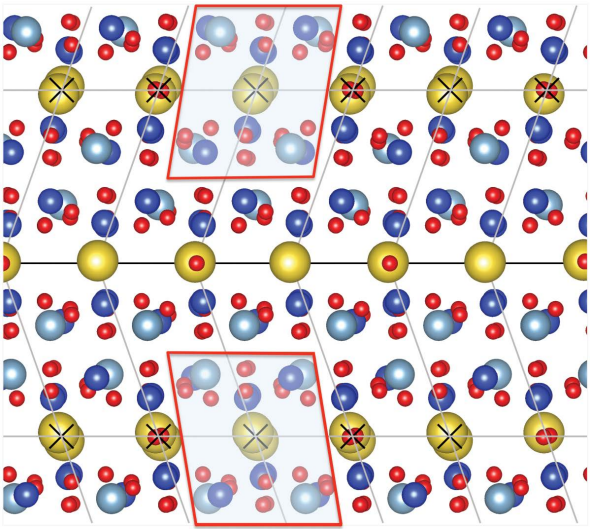

FIGURE 9. Pseudo-twin, with the anti-site defects of Figure 8 unrelaxed. (Color online.)

the even smaller local nonlinear displacements near the boundary also required thermal activation (Li and Knowles 2013).

THE IDEAL BICRYSTAL

There are several procedures to determine disconnection characteristics. The traditional scheme is to use the coherent CDP to determine **b** and h, and the CDC to find all displacements **u**. In the formation of the ideal bicrystal (the final reference space) from the CDC, these displacements are separated into **b**, **s**, and **p** vectors. This method best reflects the underlying symmetry and is preferable for simple crystals. This type of CDC is illustrated in Supplemental[1] Figure A1b.

Alternatively, one can use the SDC shifted by **b** and **p**, leaving only the SDC for the step portion of the dislocation (Hirth et al. 2016). Such a SDC is illustrated for the case where **p** is zero in Supplemental[1] Figure A1c. Only shuffles are present in this reduced SDC, as given by Equation 3. In the e-cell of the SDC, the rotation of the atomic dipole suffices to yield all shuffles. Thus, as shown here, the latter method simplifies the determination of shuffles when the crystal structure is complex. In progressing from the CDC to the SDC to the ideal bicrystal, there is a continued reduction in symmetry.

The ideal Bilby bicrystal is perfect on either side of the interface (Hirth et al. 2013). This is the space that is used in conjunction with ordinary Burgers circuits. As illustrated in Supplemental[1] Figure A1a, a dividing surface in the CDC is located midway between the last plane transformed and the next untransformed plane (Pond et al. 2016). Hence, it is displaced from the coherent interface in the CDC by $d/2$, where d is the interplanar spacing (the twin symmetry plane remains the coherent plane). Matrix atoms are removed below the dividing surface and twin planes are removed above the dividing surface, creating the Bilby bicrystal, which also has an interface displaced from atomic planes by $d/2$. This interface corresponds to the thermodynamic Gibbs interface. In this reference bicrystal, one could construct circuits around a defect to determine **b**. However, the CDC would still be needed to determine shuffles.

The real bicrystal, another representation, would have additional strains, but these would be localized to the near-interface region. These nonlinear strains are not considered here. They could be found in an atomistic simulation or possibly by atomic resolution HRTEM.

Imperfect defects

Imperfect defects are most conveniently depicted in the CDC. For such defects, the vectors analogous to $\mathbf{t}_\lambda$ do not connect the origin to a lattice site in λ: hence, they are designated as $\mathbf{q}(\lambda)$. Consequently, there is a stacking fault on one side of the defect. Equation 1 is modified to

$$\mathbf{b} = \mathbf{q}(\lambda) - \mathbf{t}(\mu). \quad (4)$$

One simple example is a ½<112> partial in a face-centered cubic (*fcc*) structure. Another is the defect observed in Al when a ⅓<111> disconnection at a twin boundary dissociated into a ⅙<111> partial and a ⅔<111> partial (Pond 1989). Such imperfect defects do not form unless the fault associated with $\mathbf{q}_\lambda$ is low in energy, which usually requires that $\mathbf{q}_\lambda$ is rational. For example, the intrinsic fault associated with a ⅙<112> partial in fcc is rational, has local symmetry and is associated with low stacking fault energy. Similar defects are found in layer structures such as graphite and mica (Amelinckx 1964). Another special type relates to CDCs with simple dipoles or multipoles at cell sites. The structural group dipole in Figure 6a is of this type. This CDC can be envisioned as two interpenetrating, simple, triclinic, structural group complexes, A (red) and B (gray). A

possible partial is one with **b** connecting an A site to a B site. Similarly, a shuffle vector could connect A and B sites. These are more likely when h is $2h_0$ or more, since the local strains accompanying shuffles decrease with increasing h. Shuffles of this type have been observed in a simulation of hcp $(11\bar{2}0)$ twinning in Zr (Khater et al. 2013). Partials of this type also have been associated with disconnections of a synchroshear type in alumina (Krönberg 1957), olivine-spinel transformations (Poirier 1981), and in Laves phases (Hazzledine and Pirouz 1993). In most cases, the glide plane or twin plane has sufficient symmetry that a given fault can be created either by glide (e.g., by a ⅙<112> partial in *fcc*) or by climb (e.g., by a ⅓<111> partial in *fcc*).

Other defects

Several other defects including disclinations (Barrett and El Khadiri 2014), facets (Li et al. 2010), interface junctions (Pond 1989), and type II twins (Pond and Hirth 2018), have been described with the TM. By applying the concept of structural groups, one can describe these defects in an identical manner to that presented here. In all cases, including the defects described in the previous sections, the kinetics of motion entails the addition of atoms at kinks or jogs on the defect lines. Discussion of the details is beyond the scope of the present treatment. For disconnections in either the phase transformation case or the twinning case, the activation energy for defect motion has contributions from shuffle motions, not simply those associated with the dislocation component.

Discussion

Much of the description here entails tractable methods for determining shuffles in complex minerals. The simpler CDP suffices to define **b**, h, and the shear accompanying twinning. The complete description of a disconnection entails the shuffles (**s**) as well. Understanding the shuffles is essential in determining the most likely disconnection for a given twin and in modeling disconnection motion (twin growth). The basic concept, incorporated in the TM, is that the most likely disconnection is that with the shortest set of shuffle vectors (Bilby and Crocker 1965; Christian and Mahajan 1995). For albite, we see that the determination of shuffle vectors is greatly simplified if one first removes the shuffles associated with the structural groups (which removes effects associated with **b** and **p**), and then uses the SDC to determine the remaining shuffles. Our analysis also demonstrates the possibility (likelihood) of large steps with many shuffles, based on the requirement for switching of atoms from Si and Al sites; the application of these techniques for twinning in plagioclase solid-solution phases could involve similar steps related to switching between Ca-Na sites.

The major focus of the mechanistic applications of the TM has been on phase transformations and twinning. There are other disconnection models and mechanisms with many similarities. In particular we note the extensive work on grain boundary sliding (e.g., Rajabzadeh et al. 2014; Combe et al. 2016; Han et al. 2018), a process that has been interpreted to be important for several geologic materials, including olivine (e.g., Hansen et al. 2011), calcite (e.g., Austin et al. 2014), plagioclase (Miranda et al. 2016), and quartz (Cross et al. 2017). In all of these applications, the reference lattices provide the basis for the application of the TM to all disconnection models. While earlier work emphasized the importance of interface steps for phase transformations (e.g., Howe and Smith 1992), twinning (e.g., Hardouin Duparc 2017), and grain boundary sliding (e.g., Langdon 2006), the formal description of the TM is not trivial (Hirth et al. 2013; Han et al. 2018). Long-range fields are associated with the Burgers vector for dislocation components or the Frank vector for disclination components. The motion of the step component produces pure rotation related to disclination quadrupoles. Similarly, the reference spaces of the TM describe spacing defects, line forces, and non-equilibrium structures. The motion of the step component produces pure rotation related to disclination quadrupoles.

We emphasize that the shuffles found in the reference spaces of the TM are important in describing the mechanism of disconnection motion, e.g., in twin growth. In atomistic simulations of twin growth, it is important to determine the height and Burgers vector (or Frank vector) for the most likely disconnection In this case, for a given growth rate the twin stress can be predicted. In one example, only the TM accurately predicts the geometry of a type II twin (Pond et al. 2018). Many researchers are employing disconnections and advancing new ideas, mainly for simple structures. In all cases, the concept of structural groups would be a useful tool for the extension of this body of work to complex minerals.

The topic of disconnections is a burgeoning field. We anticipate that there will be many applications for minerals. We have given one example of twinning for low albite. The twin methodology should be important in the computer simulation of deformation twin growth, and in modeling dislocation-twin intersections. The same TM methodology can be applied to order-disorder transformations, phase changes, slip, defect-boundary interactions, and boundary details such as facets. The TM concepts described here can serve as a template to analyze these processes as well. What we have emphasized here is that the analysis of structural aspects of disconnections, most importantly shuffling, can be simplified by treating unit cells of complex structures comprised of structural groups.

Implications

The model presented here describes the mechanism for deformation twinning and applies as well to shear-type transformations and grain boundary deformation. We chose to illustrate the model for twinning in albite owing to its potential application for constraining the rheological properties of the crust at conditions near the brittle-plastic transition, where plagioclase is a major constituent of common rock types. While deformation twins in plagioclase are often described from microstructural analyses in crustal rocks, the interpretation of the stress states at which they form has not advanced partly owing to difficulties in quantifying constitutive laws. The concept of structural groups makes an analysis of the twinning transformation process easier in complex minerals and explicitly predicts the interface structure of the deformation twins. Twinning is particularly important at lower temperatures, where creep by diffusional relaxation is limited and large stress concentrations arise at triple points and near grain boundaries. At these conditions dislocation slip in plagioclase becomes limited, partly because of the large Burgers vectors. Twinning then becomes a possible mechanism to satisfy the von

Mises requirement and to accommodate stress concentrations. Recent advances in microscopy (e.g., high-angular resolution electron backscatter diffraction, Wallis et al. 2016) presage new analyses of twinning in feldspars (as well as other minerals) that could be used to investigate stress states at these conditions, in addition to the role of crystal plasticity during semi-brittle flow and fracture near the base of the seismogenic zone and in regions near impacts.

Atomistic simulation of deformation is a burgeoning field. For twinning simulations, the TM analysis is useful in providing the likely twinning disconnection and the proper boundary conditions. The shear and the shuffles provide a basis for analyzing the activation energy (including the stress dependence) for twin growth, important in developing constitutive relations for deformation, which in turn provide input for analyzing the microstructure of polycrystals. This is important because twins created in the laboratory can form at rates up to eight orders of magnitude faster and have twin sizes two or three orders of magnitude smaller than those formed naturally. Thus, if the interface structures observed in high-resolution electron microscopy are the same for both laboratory and natural structures, then constitutive relations for deformation (determined in the laboratory) should also apply to the natural twins. Knowledge of the constitutive relations enables one to know the critical stress and temperature for the twinning-slip transition. Disconnection concepts apply directly to grain boundary sliding and twinning and would also be essential in developing constitutive relations for these processes.

Acknowledgments and Funding

The authors are pleased to acknowledge helpful contributions by R.C. Pond, in particular for symmetry considerations, by Sylvie Demouchy, John Wheeler, and by Dongyue Xie. Jian Wang acknowledgments support from the U.S. National Science Foundation (NSF) (CMMI-1661686). Greg Hirth acknowledges support from NSF (EAR-1624178).

References cited

Amelinckx, S. (1964) The Direct Observation of Dislocations. Solid State Physics Supplement 6. Academic Press.

Anderson, P.M., Hirth, J.P., and Lothe, J. (2017) Theory of Dislocations, 3rd ed., 699 p. Cambridge University Press.

Austin, N., Evans, B., Rybacki, E., and Dresen, G. (2014) Strength evolution and the development of crystallographic preferred orientation during deformation of two-phase marble. Tectonophysics, 631, 14–28.

Barrett, C.D., and El Khadiri, H. (2014) The roles of grain boundary dislocations and disclinations in the nucleation of $\{10\bar{1}2\}$ twinning. Acta Materialia, 63, 1–15.

Bilby, B.A., and Crocker, A.G. (1965) The theory of the crystallography of deformation twinning. Proceedings of the Royal Society (London) A, 288, 240–255.

Christian, J.W., and Mahajan, S. (1995) Deformation twinning. Progress in Materials Science, 39, 1–157.

Combe, N., Mompiou, F., and Legros, M. (2016) Disconnections kinks and competing modes in shear-coupled grain boundary migration. Physical Review B, 93, 024109, 1–6.

Cross, A.J., Hirth, G., and Prior, D.J. (2017) Effects of secondary phases on crystallographic preferred orientations in mylonites, Geology, 45, 955–958.

Hahn, T., and Klapper, H. (2006) Twinning of crystals. International Tables for Crystallography Volume D: Physical properties of crystals, p. 393–448. Springer, Dordrecht.

Han, J., Thomas, S.L., and Srolovitz, D.J. (2018) Grain-boundary kinetics: A unified approach. Progress in Materials Science, 98, 386–476.

Hansen, L.N., Zimmerman, M.E., and Kohlstedt, D.E. (2011) Grain boundary sliding in San Carlos olivine: Flow law parameters and crystallographic-preferred orientation. Journal of Geophysical Research, 116. https://doi.org/10.1029/2011JB008220

Hardouin Duparc, O.B.M. (2017) A review of some elements for the history of mechanical twinning centred on its German origins until Otto Mügge's K1 and K2 invariant plane notation. Journal of Materials Science, 52, 4182–4196.

Hazzledine, P.M., and Pirouz, P. (1993) Synchroshear transformations in Laves phases. Scripta Metallurgica, 28, 1277–1282.

Hirth, J.P., and Pond, R.C. (1996) Steps, dislocations and disconnections as defects relating to structure and phase transformations. Acta Materialia, 44, 4749–4763.

Hirth, J.P., Pond, R.C., Hoagland, R.G., Liu, X.Y., and Wang, J. (2013) Interface defects, reference spaces and the Frank-Bilby equation. Progress in Materials Science, 58, 749–823.

Hirth, J.P., Wang, J., and Tomé C.N. (2016) Disconnections and other defects associated with twin interfaces. Progress in Materials Science, 83, 417–471.

Howe, J.M., and Smith, D.A. (1992) Comparison between the invariant line and structural ledge theories for predicting the habit plane, orientation relationship and interface boundary structure of plate-shaped precipitates, Acta Metallurgica et Materialia, 40, 2343–2350.

Howe, J.M., Pond, R.C., and Hirth, J.P. (2009) The role of disconnections in phase transformations. Progress in Materials Science, 54, 792–838.

Khater, H.A., Serra, A., and Pond, R.C. (2013) Atomic shearing and shuffling accompanying the motion of twinning disconnections in zirconium. Philosophical Magazine, 93, 1279–1298.

Krönberg, M.L. (1957) Plastic deformation of single crystals of sapphire: Basal slip and twinning. Acta Metallurgica, 5, 507–524.

Langdon, T.G. (2006) Grain boundary sliding revisited. Journal of Materials Science, 46, 597–609.

Li, B., and Knowles, K.M. (2013) Molecular dynamics simulation of albite twinning and pericline twinning in low albite. Modelling and Simulation in Materials Science and Engineering, 21, 05501.

Li, Y.J., Chen, Y.J., Walmsley, J.C., Mathinsen, R.H., Dumoulin, S., and Roven, H.J. (2010) Faceted interfacial structure of {1011} twins in Ti formed during equal channel angular pressing. Scripta Materialia, 62, 443–446.

Medlin, D.L., and Yang, N.Y.C. (2012) Interfacial step structure at a (0001) basal twin in Bi_2Te_3. Journal of Electronic Materials, 41, 1456–1464.

Miranda, E.A., Hirth, G., and John, B.E. (2016) Microstructural evidence for the transition from dislocation creep to dislocation-accommodated grain boundary sliding in naturally deformed plagioclase. Journal of Structural Geology, 92, 30–45.

Poirier, J.P. (1981) On the kinetics of olivine-spinel transition. Physics of the Earth and Planetary Interior, 26, 179–187.

Pond, R.C. (1989) Line defects in interfaces. In F.R.N. Nabarro, Ed., Dislocations in Solids, vol. 8, 5–66. Elsevier.

Pond, R.C., and Hirth, J.P. (1994) Defects at surfaces and interfaces. Solid State Physics, 47, 287–365.

——— (2018) Topological model of type II deformation twinning. Acta Materialia, 151, 229–242.

Pond, R.C., and Vlachavas, D.S. (1983) Bicrystallography. Proceedings of the Royal Society (London), 386A, 95–143,

Pond, R.C., Ma, X., Chai, Y.W., and Hirth, J.P. (2007) Topological modelling of martensitic transformations. In F.R.N. Nabarro and J.P. Hirth, Eds., Dislocations in Solids, 13, p. 225–262. Elsevier.

Pond, R.C., Hirth, J.P., Serra, A., and Bacon, D.J. (2016) Atomic displacements accompanying deformation twinning: shears and shuffles. Materials Research Letters, 5, 541–544.

Rajabzadeh, A., Mompiou, F., Lartigue-Korinek, S., Combe, N., Legros, M., and Molodov, D.A. (2014) The role of disconnections in deformation-coupled grain boundary migration. Acta Materialia, 77, 223–235.

Ribbe, P.H. (1974) Crystal structure and physical properties. In Feldspar Minerals, vol. 1, 1–19. Springer-Verlag.

Wallis, D., Hansen, L.N., Britton, T.B., and Wilkinson, A.J. (2016) Geometrically necessary dislocation densities in olivine obtained using high-angular resolution electron backscatter diffraction. Ultramicroscopy, 168, 34–45.

Wenk, H.-R., and Bulakh, A. (2016) Minerals: Their Constitution and Origin. Cambridge University Press.

Manuscript received November 13, 2018
Manuscript accepted March 18, 2019
Manuscript handled by Sylvie Demouchy

Endnote:

[1]Deposit item AM-19-76892, Appendix A. Deposit items are free to all readers and found on the MSA website, via the specific issue's Table of Contents (go to http://www.minsocam.org/MSA/AmMin/TOC/2019/Jul2019_data/Jul2019_data.html).